sustainability

MDPI

Article

A Sustainable Superhydrophobic and Photothermal Coatings for Anti-Icing Application on Concrete with a Simple Method for CNTs/SiO_2 Modification

Shuai Li [1], Yanwei Li [2,3], Yiqiu Tan [1,4,*], Jilu Li [1], Di Wang [5], Dongdong Yuan [6] and Jianli Zhang [2,3]

1 School of Transportation Science and Engineering, Harbin Institute of Technology, Harbin 150090, China; lischd@163.com (S.L.); lijiluhit@163.com (J.L.)
2 Hebei Provincial Communications Planning and Design Institute, Shijiazhuang 050090, China
3 Research and Development Center of Transport Industry of Technologies, Materials and Equipments of Highway Construction and Maintenance, Shijiazhuang 050090, China
4 State Key Laboratory of Urban Water Resource and Environment, Harbin Institute of Technology, Harbin 150090, China
5 Department of Civil Engineering, Aalto University, 02150 Espoo, Finland; di.1.wang@aalto.fi
6 School of Highway, Chang'an University, Xi'an 710064, China; ddy@chd.edu.cn
* Correspondence: tanyiqiu@hit.edu.cn

Abstract: Ice formation on concrete surfaces significantly challenges productivity, economic growth, and safety in diverse industrial sectors. Superhydrophobic coatings represent an effective solution to delay ice formation, although their functionality deteriorates under repeated freeze–thaw cycles. To address this issue, carbon nanotubes (CNTs) are frequently employed due to their exceptional photothermal conversion and mechanical properties, which contribute to extending the sustainability of the superhydrophobic coatings. However, the chemical inertness of CNTs often necessitates complex reactions to modify their functionalization. In this study, we have invented a simple method involving the sequential growth of silica on the surface of CNTs and the hydrophobic modification of the silica surface to enhance CNT functionality. These CNTs/SiO_2 functionalized nanoparticles were then incorporated into an epoxy resin using a simple spray technique, resulting in a superhydrophobic and photothermal coating on concrete. To fine-tune the coating's properties, we explored the effects of varying the doping levels of the nanoparticles on the surface morphology, roughness, and wettability of the CNT/SiO_2-EP coatings. The optimal level of hydrophobicity was achieved by doping the coatings with 300 mg of functionalized nanoparticles, yielding an impressive contact angle of 159.6°. The integration of functionalized nanoparticles into the epoxy matrix not only enhances hydrophobicity but also improves mechanical robustness and abrasion resistance by creating multiscale surface roughness. Additionally, the coating exhibits outstanding chemical stability even under extreme conditions. One of the most significant advantages of these coatings is their ability to extend the ice nucleation time significantly. This effect is primarily attributed to the superior superhydrophobicity of the nanoparticles and the remarkable photothermal conversion capability of the CNTs. Upon exposure to Xenon lamp radiation, the ice droplets rapidly melt, underscoring the impressive performance of these coatings in preventing ice formation.

Keywords: superhydrophobic; photothermal; anti-icing; carbon nanotubes; concrete; silica

Citation: Li, S.; Li, Y.; Tan, Y.; Li, J.; Wang, D.; Yuan, D.; Zhang, J. A Sustainable Superhydrophobic and Photothermal Coatings for Anti-Icing Application on Concrete with a Simple Method for CNTs/SiO_2 Modification. *Sustainability* **2023**, *15*, 15865. https://doi.org/10.3390/su152215865

Academic Editor: Zhibin Ye

Received: 26 September 2023
Revised: 22 October 2023
Accepted: 8 November 2023
Published: 12 November 2023

1. Introduction

Concrete is a fundamental material in infrastructure, from roadways and bridges to architectural constructions [1–4]. However, its porous and hydrophilic nature can lead to issues with water absorption and freezing in cold winter climates, which can compromise slip resistance on concrete pavements and cause traffic accidents [5–8]. Furthermore, freeze–thaw cycles within concrete structures can result in structural damage [9]. De-icing methods fall into two main categories: active and passive approaches [10,11]. Active methods

involve mechanical techniques, chemical solvent applications, and electro-thermal methods. Unfortunately, these methods often consume significant energy and require specialized equipment, limiting their practicality. On the other hand, passive de-icing strategies aim to delay and inhibit ice formation. These include ice-resistant hydrogel surfaces, bio-mimetic ice-resistant surfaces, and superhydrophobic surfaces [12–15]. Although these methods have shown resistance to icing under certain conditions, there are still limitations.

Superhydrophobic surfaces featuring micro-nano structures effectively remove water droplets during condensation. This capability delays ice nucleation and reduces ice accumulation [16,17]. However, the limited sustainability, intricate preparation process, and monotonous functionality of superhydrophobic coatings restrict the potential applications. The primary factor contributing to the inadequate sustainability of superhydrophobic coatings is that the micro-nano structure on the coating's surface is vulnerable to damage from friction and impact [18,19]. Various strategies have been explored to enhance the limited sustainability of these coatings. Kwak et al. conducted composite modifications on silicon dioxide and titanium dioxide, employing various processing methods to apply superhydrophobic coatings with multiple micro-nano structures. These coatings are versatile and demonstrate exceptional durability on a range of substrate surfaces [20]. Lahiri et al. employed Polydimethylsiloxane (PDMS) as a binder to affix H_3BO_3 and SiO_2 nanoparticles to the substrate surface, resulting in a highly durable superhydrophobic coating. Remarkably, even after undergoing 40 peeling experiments, it retained hydrophobic properties [21]. However, when exposed to extended freezing conditions, the micro-nano structure establishes a mechanical interlocking connection with ice, thereby intensifying the adhesion between the ice and the coated surface.

Sunlight-induced heat can substantially elevate the surface temperature of objects, serving as the most basic and straightforward anti-icing method. Photothermal materials, possessing efficient photothermal conversion properties, offer a solution to the challenge of ice adhesion without causing harm to the micro-nano structures on the surface of superhydrophobic coatings [22–24]. Liu et al. fabricated a dual-layered photothermal material using a spray coating process. This material comprised sparsely coated fluorinated multi-walled carbon nanotubes (CNTs) and polyurethane. The heat generated within the photothermal layer efficiently propagated across the coating's surface via the conductive layer. However, thermal transmission to the substrate was limited by a thermal protection layer. Notably, outdoor experiments showcased the remarkable effectiveness of this coating in preventing ice formation [25]. Inspired by the structural features of wheat blades, Zhang et al. developed a highly efficient photothermal anti-icing/frost coating through ultrafast pulsed laser deposition (UFPD). This coating demonstrated exceptional capabilities for self-removal of water droplets and efficient photothermal conversion, especially in challenging environmental conditions characterized by low temperature and high humidity. The coating excels in self-removal of water droplets and exhibits outstanding photothermal conversion efficiency, even in low temperatures and high humidity. Moreover, it offers the flexibility to be applied to various substrates while maintaining robust durability and adaptability [26].

Carbon nanotubes (CNTs) show great promise as ideal candidates for creating superhydrophobic coatings owing to their versatile structure and impressive mechanical properties [27–29]. However, the weak interfacial bonds and uneven dispersion of CNTs within organic polymers have posed challenges in improving the mechanical strength of these coatings. Therefore, innovative composite configurations are essential to enhance CNT-based superhydrophobic coatings, ensuring better dispersion and mechanical durability [30–32]. Zhang et al. prepared a CNTs-SiO_2 hybrid by grafting carbon nanotubes (CNTs) onto silica nanoparticles through complex chemical reactions and then incorporated it into epoxy resin to construct a superhydrophobic coating through the spraying method. Upon exposure to 808 nm laser irradiation, the surface temperature of the coating experiences a swift increase, leading to the rapid melting of condensed ice. Liu et al. introduced a simple surface modification technique for carbon nanotubes (CNTs). This method entails applying

a dopamine layer onto the CNTs' surface and linking the active and hydrophobic groups present on the dopamine surface. This process results in the creation of CNT nanoparticles with superhydrophobic properties [10]. While current methods can achieve hydrophobic modification of CNTs, challenges such as complex reaction processes or high costs are often encountered.

In this work, we present a novel and uncomplicated approach for modifying CNTs-SiO_2 nanoparticles through the sequential growth of SiO_2 on the surface of CNTs. The modifying CNTs-SiO_2 nanoparticles are termed "functionalized nanoparticles". Using a straightforward spraying method, we produced superhydrophobic photothermal coatings based on these functionalized nanoparticles. Our investigation focused on the influence of the doping amount of functionalized nanoparticles on the coatings' surface morphology, wettability, and photothermal properties. We identified the rough micro- and nanostructures on the coatings and evaluated their chemical stability under challenging pH conditions, such as highly acidic and alkaline environments. To assess their mechanical robustness, we conducted tape peeling and friction tests. Our findings revealed that the introduction of functionalized nanoparticles led to the formation of micro- and nanostructures at various scales on the coatings' surface, with agglomeration and interlocking effects between nanoparticles enhancing the coatings' mechanical durability. Moreover, the CNTs-SiO_2/epoxy coating demonstrated efficient droplet melting under simulated solar irradiation, thanks to the superior water repellency of the coated surface and the photothermal conversion capabilities of the CNTs. Combining the anti-icing and de-icing properties of CNTs-SiO_2/epoxy coatings can significantly expand the practical applications of superhydrophobic coatings.

2. Materials and Methods

2.1. Materials

Ethyl orthosilicate (TEOS), hexadecyltrimethylammonium bromide (CTAB), ammonia water, perfluorodecyltrichlorosilane (PDTS), all of which were purchased from McLean Biochemical Technology Co., Ltd., Shanghai, China. CNTs were purchased from Jiazhaoye New Materials Co., Ltd. (Shenzhen, China). Anhydrous ethanol was purchased from Longbohua Co., Ltd. (Tianjin, China). Waterborne epoxy resin and curing agent were purchased from Runxiang Chemical Co., Ltd. (Qingdao, China) as binders.

2.2. Preparation of Functionalized Nanoparticles

Figure 1 illustrates the process for achieving hydrophobic modification of CNTs-SiO_2. The procedure commenced with the dispersion of 0.5 g of CTAB in 100 mL of deionized water, followed by ultrasonication until the solution became clear. Subsequently, 1 g of CNTs was introduced into the solution and subjected to 30 min of ultrasonication. Then, 1 mL of ammonia and 3 mL of TEOS solution were added dropwise into the mixture, which was magnetically stirred at room temperature for 6 h. The resulting nanoparticles underwent a washing and drying process, repeated twice, to yield CNTs coated with silica. Following this, the nanoparticles underwent hydrophobic modification. Initially, 0.5 g of CNTs-SiO_2 nanoparticles were dispersed in 100 mL of anhydrous ethanol. After ultrasonic dispersion for 5 min, 3 mL of PDTS was added to the solution, which was then magnetically stirred at 60 °C for 3 h. The steps of material addition are delineated as Steps 1, 2, and 3 in Figure 1. The resulting nanoparticles were subjected to repeated washing and drying cycles with deionized water and alcohol, forming CNTs-SiO_2 nanoparticles with superhydrophobic properties, hereafter referred to as "functionalized nanoparticles".

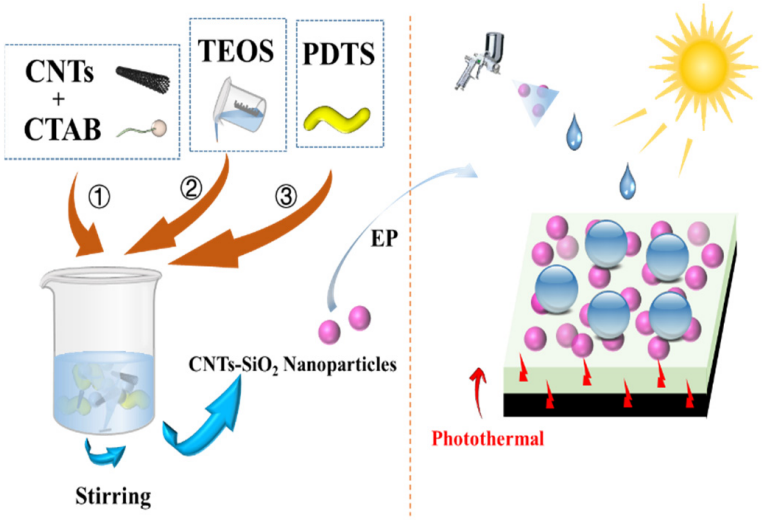

Figure 1. Preparation process of functionalized particles and superhydrophobic coatings.

2.3. Preparation of Composite Coatings

In the experiment, the functionalized nanoparticles with different masses of 100 mg, 300 mg, and 500 mg were, respectively, added to acquire coatings with a resin content of 98%, 94%, and 90%, labeled as CS1-E, CS3-E, and CS5-E. These solutions were subjected to ultrasonic dispersion for 10 min. Subsequently, a water-based epoxy resin curing agent was introduced, and the combination was magnetically stirred at room temperature for 30 min to create a homogeneous suspension. This uniform material suspension was then sprayed onto the surface of cement concrete specimens using specific conditions, including 0.5 MPa of compressed air, a spraying time of 5 s, and a distance of 15 cm between the specimen and the spray gun. After spraying, the sample was cured in a blast drying oven at 80 °C for 2 h, successfully producing a coating on the concrete surface. The preparation procedure is depicted in Figure 1.

2.4. Characterization

Transmission electron microscopy (TEM, JEM-1400, JEOL, Tokyo, Japan) was used to examine the surface morphology of functionalized nanoparticles. Fourier infrared spectroscopy (Nicolet is50 FT-IR) analyzed their chemical bond compositions with a 4000–500 cm^{-1} scanning range. Thermal stability was tested using a thermogravimetric analyzer (TGA, STA449F3, NETZSCH, Selb, Germany) with a test score of N_2 and a temperature of 30–800 °C. After the coating preparation, the surface morphology of the coating was observed by scanning electron microscope (SEM, SIGMA-500, ZEISS, Oberkochen, Germany), and the roughness of the coating was observed using three-dimensional confocal microscope (CLSM, OLS3000, OLYMPUS, Tokyo, Japan).

2.5. Contact Angle Test

Droplet contact angle and roll angle measurements were carried out using the Dataphysics OCA20 contact angle tester. To determine the contact angle, a 10 µL droplet was meticulously placed on the material's surface, and its contact angle was measured. For the rolling angle test, the procedure began with a 0° starting angle and was incrementally raised by 1° until the droplet initiated rolling down the surface. This incremental increase in angle was continued until rolling occurred. Each group conducted five parallel tests to ensure the precision and consistency of the test results. This approach involved multiple measurements to generate reliable and accurate data.

2.6. Mechanical Durability

The mechanical toughness of the coating was assessed via a tape peeling test. In this test, a specific type of tape was firmly affixed to the coated surface using 30 kPa of pressure.

Afterward, the tape was systematically removed from the surface. To evaluate the coating's adhesion and resistance to tape peeling, this peeling process was repeated 200 times.

2.7. Anti-Icing and De-Icing Experiments

To assess the photothermal conversion capabilities of the coating when exposed to light, a 1 kW/m^2 Xenon lamp was utilized. An infrared thermographer was employed to monitor and record changes in the surface temperatures of the coatings. These experiments were conducted in a controlled environment within a cold box, which allowed for precise temperature regulation to manipulate environmental factors. The cold box was adjusted to −10 °C, creating a rigorously cold testing environment. Furthermore, relative humidity was carefully controlled, maintaining it at 35 ± 5% with a humidifier. Throughout the testing process, the distance between the light source spot and the coating surface was consistently maintained at 15 cm. This carefully controlled experimental setup was designed to simulate and evaluate the photothermal performance of the coatings under specific environmental conditions.

3. Results and Discussion

3.1. Characterization of Functionalized Nanoparticles

The surface modification of CNTs commenced with CTAB, a compound possessing both hydrophilic and hydrophobic groups. These groups were strategically oriented with the hydrophilic segments facing the solution, while the hydrophobic sections were directed inward, forming a template structure through self-assembly. Subsequently, when TEOS, the repellent agent, was introduced into the solution under alkaline conditions, it underwent hydrolysis, generating silicate ions that electrostatically interacted with the CTAB micelles. These silicate ions were deposited along the CTAB, forming a silica layer that enveloped the surface of the CNTs, ultimately creating a composite structure. This process effectively counteracted van der Waals forces between the CNTs, improving their dispersion within the matrix. Moreover, the abundance of -OH groups on the silica's surface significantly increased the opportunities for functionalizing CNTs, overcoming their inherent surface inertness. Subsequently, hydrophobic modification of the functionalized nanoparticles was achieved through the hydrolysis of PDTs, enabling grafting modifications on the numerous hydroxyl groups on the silica's surface. Figure 2 provides a transmission electron microscope (TEM) image of the functionalized nanoparticles, vividly illustrating the successful and uniform coating of silica onto the CNTs. The silica grew uniformly along the CNTs, forming a distinct core–shell structure with excellent bonding. Initially, the diameter of the CNTs measured 15–20 nm, whereas the diameter of the functionalized nanoparticles expanded to 35–40 nm after the silica coating process.

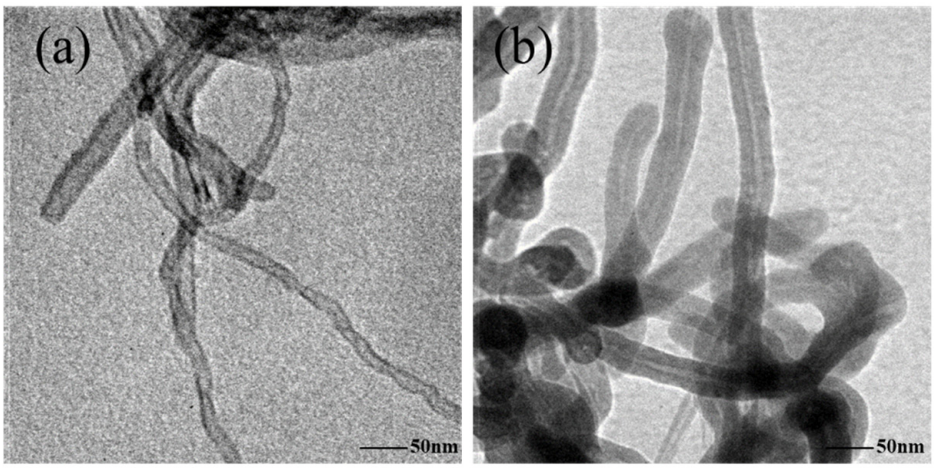

Figure 2. TEM images of (**a**) CNTs and (**b**) functionalized nanoparticles.

The chemical structures of the CNTs were analyzed using FT-IR, and Figure 3 presents the infrared spectra of CNTs, SiO_2, and the functionalized nanoparticles. Within these spectra, several significant absorption peaks are noteworthy. At 955 cm^{-1}, absorption peaks indicate the expansion and contraction vibrations of the Si-O-Si bond, consistent with pure silica characteristics. Furthermore, at 1625 cm^{-1}, there is an absorption peak corresponding to the stretching vibrations of the C=C bond, a distinctive feature of CNTs. The presence of -OH stretching vibrations at 3390 cm^{-1} suggests a substantial number of -OH groups on the SiO_2 surface [33]. In addition to these peaks, the absorption peaks at 2866 cm^{-1}, 2613 cm^{-1}, and 1430 cm^{-1} are associated with the presence of PDTs and CTAB in the sample. Smaller absorption peaks at 561 cm^{-1}, 632 cm^{-1}, and 681 cm^{-1} can be attributed to the bending vibrations of the C-N bond in CTAB. A notable peak at 563 cm^{-1} is linked to the vibration of the C-Br bond [34]. Interestingly, a new distinctive peak at 1375 cm^{-1} has emerged, which is attributed to the vibration of the F-C bond [35]. These FT-IR results offer valuable insights into the chemical composition and bonding within the functionalized nanoparticles, affirming the successful modification and the coexistence of various functional groups within the composite material.

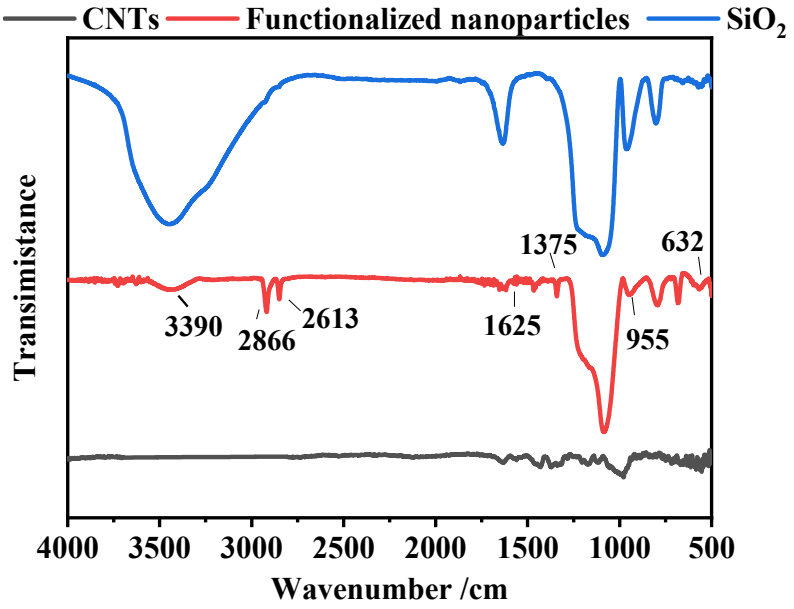

Figure 3. FTIR spectra of different materials.

As illustrated in Figure 4, the curves representing CNTs and SiO_2 show relatively shallow and minor peaks. In the temperature range from 100 to 600 °C, CNTs experience a mass loss of approximately 5.1%, while SiO_2 undergoes a slightly higher mass loss of about 7.2%. This initial mass loss can mainly be attributed to trace impurities in the materials and water molecules adsorbed within the testing chamber. Regarding the functionalized nanoparticles, the mass loss in the temperature range from 100 to 200 °C is relatively modest and primarily results from the evaporation of impurities and adsorbed water molecules. However, as the temperature rose, a significant mass reduction was observed from 200 °C to 400 °C. Beyond this temperature range, the mass stabilizes, resulting in an overall mass loss of 18.5%. Notably, this 11.3% difference in mass reduction compared to SiO_2 can be ascribed to the decomposition and polymerization of the CTAB and PDTS groups in the hybrids. These observations yield valuable insights into the hybrid material's thermal behavior and decomposition patterns, shedding light on the presence of specific functional groups and their reactions under varying temperature conditions.

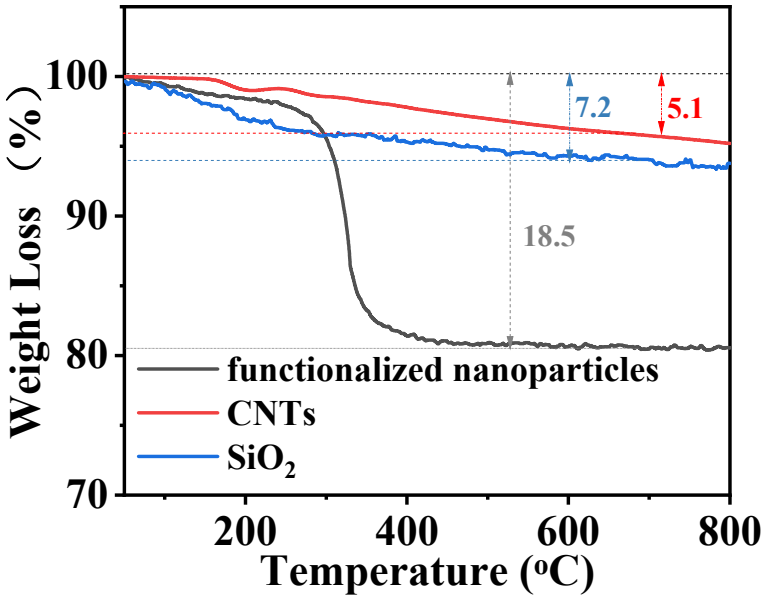

Figure 4. TGA curves of CNTs, functionalized nanoparticles, and SiO_2.

3.2. Surface Properties of Coatings

The versatility of these coatings is further amplified by blending functionalized nanoparticles with epoxy resin to create CNTs/SiO_2/EP coatings using a straightforward spray application technique. The surface morphology of epoxy coatings derived from CS1-E, CS3-E, and CS5-E was evaluated via scanning electron microscopy (SEM), leading to the following insights. As depicted in Figure 5, all coating surfaces were covered with micro- and nanoscale aggregates. However, there were slight variations in morphology depending on the ratio of functionalized nanoparticles to epoxy resin. In the case of CS1-E, the coating surface exhibited fewer aggregates, and some of the micro- and nanoparticles were encapsulated within the epoxy resin. Conversely, the CS3-E coating displayed a more pronounced presence of micro- and nanostructures, along with higher levels of aggregation. The CS5-E coating exhibited even larger aggregates on its surface. It is worth noting that the amount of functionalized nanoparticles in the mixture can influence the hydrophobicity and mechanical characteristics of these composite coatings. Confocal laser scanning microscopy (CLSM) images of the coatings are presented in Figure 5d–f to provide a more detailed perspective. In Figure 5d, the CS1-E coating featured randomly distributed micro- and nanostructured microscale protrusions, resulting in a surface roughness of approximately 87 μm. Conversely, the CS5-E coating exhibited a higher density of protrusions, which increased the surface roughness to around 135 μm. This increase can be attributed to the higher doping ratio of functionalized nanoparticles in the epoxy resin. Consequently, more hybrids became exposed on the coating surface, and these hybrids tended to aggregate within the coating. With a further increase in the doping of hybrids in the CS5-E coatings, the tightly packed excess SiO_2 particles produced a more uniformly arranged set of protrusions. This led to a slight reduction in surface roughness to approximately 102 μm. These findings indicate that the surface morphology and roughness of coatings can be tailored by adjusting the proportion of functionalized nanoparticles to epoxy resin, which can, in turn, impact the coatings' properties and performance.

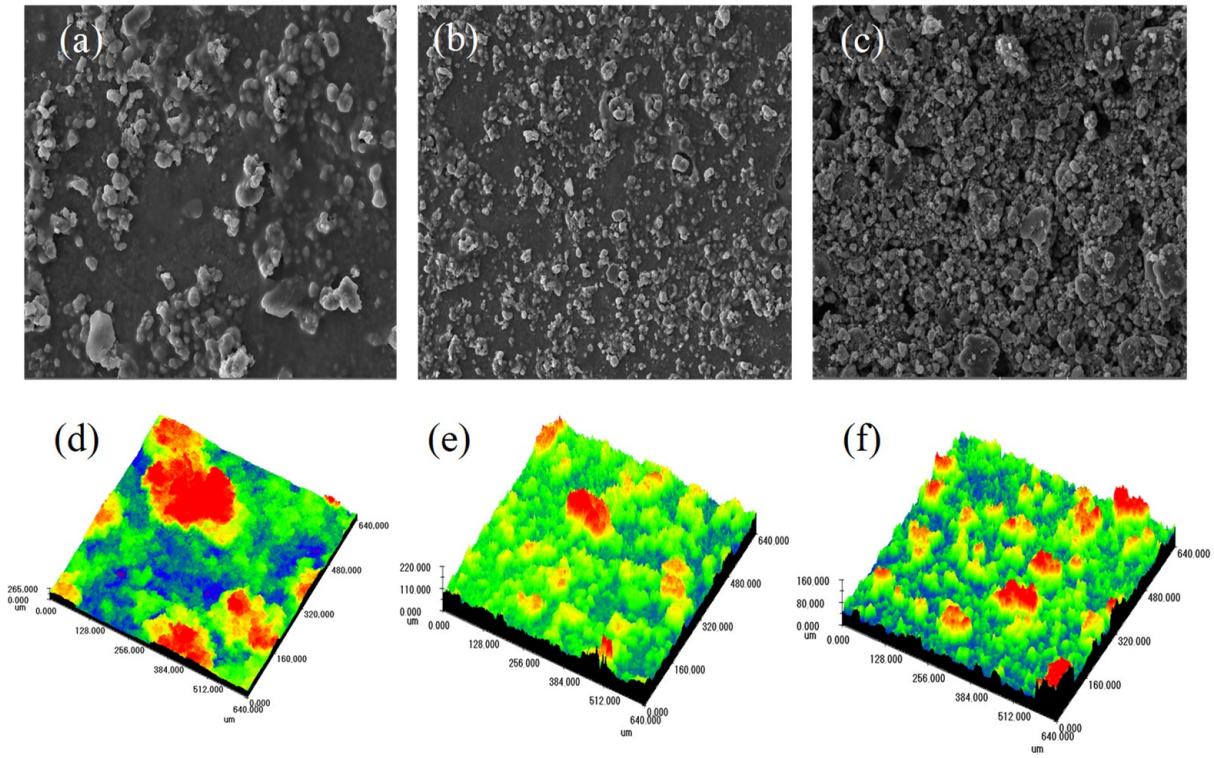

Figure 5. SEM images of (**a**) CS1-E, (**b**) CS3-E, and (**c**) CS5-E; CLSM images of (**d**) CS1-E, (**e**) CS3-E, and (**f**) CS5-E.

3.3. Superhydrophobicity of the Coatings

The Cassie–Baxter model emphasizes that micro- and nanostructures at various scales and the materials' low surface energy are pivotal factors for crafting superhydrophobic coatings. This model underscores the importance of micro- and nanostructures and low surface energy in superhydrophobic coating construction. Figure 6 shows the contact angles of superhydrophobic coatings with varying amounts of functionalized nanoparticle doping. The contact angles at all three doping levels exceeded 150°, demonstrating superhydrophobic solid properties. The maximum contact angle reached 159.6° when the yield was 300 mg. Additionally, Figure 6 provides a schematic representation of the mechanism behind the differences in contact angle size on various coatings. These coatings' micro- and nanostructures, coupled with their low surface energy attributes, promote the formation of air cushions, significantly reducing the contact area between droplets and the coating surface. Notably, the CS3-E coating featured micro- and nanostructures of an optimal size, owing to nanoparticle agglomeration and bulging, which enhanced overall roughness and ensured optimal hydrophobicity. In contrast, the CS1-E and CS5-E coatings exhibited either insufficient or excessive nanoparticle additions, resulting in altered micro- and nanostructures. This, in turn, diminished the coating's roughness and its ability to form an air cushion, consequently reducing the contact area between droplets and the surface [36,37]. As a result, the CS3-E coating was selected for further evaluation in subsequent studies.

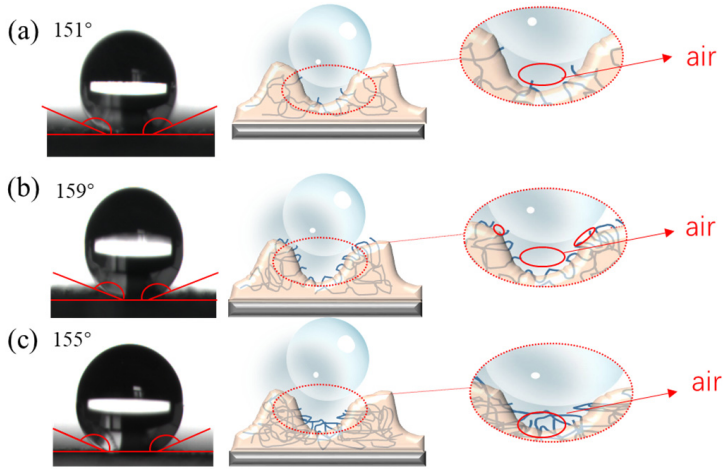

Figure 6. Schematic diagram of contact angle and mechanism of coatings: (**a**) CS1-E, (**b**) CS3-E, and (**c**) CS5-E.

3.4. Stability of Coatings

To ensure the practical applicability of superhydrophobic coatings in diverse environments, it is imperative that these coatings demonstrate robust stability. In this study, we subjected the coatings to various pH solutions, simulating extreme conditions and evaluating their chemical stability. Solutions spanning from pH 1 to pH 13 were prepared by adjusting the pH using HCl and NaOH. Subsequently, droplets were deposited onto the coating surfaces, and contact angles were measured. As illustrated in Figure 7a, the contact angles consistently exceeded 150° across the entire pH range, from 1 to 13. Furthermore, the rolling angle remained below 10°, confirming the superhydrophobic nature of the coatings. These results underscore the coatings' exceptional resistance to both acidic and alkaline environments. In further tests designed to replicate extreme conditions, the coated panels were fully immersed in solutions with varying pH levels, including HCl (pH = 1), deionized water (pH = 7), and NaOH (pH = 13). Hydrophobic angles of the coatings were measured at regular intervals (every 3 h). As depicted in Figure 7b, even after 24 h of immersion in these extreme environments, the hydrophobic angles of the coatings consistently remained above 150°. This robust performance conclusively establishes the remarkable chemical stability of the coatings. These experiments demonstrate that the CS3-E coating is exceptionally well-suited for deployment in extreme environments characterized by strong acids and alkalis, further underscoring its potential versatility and practicality.

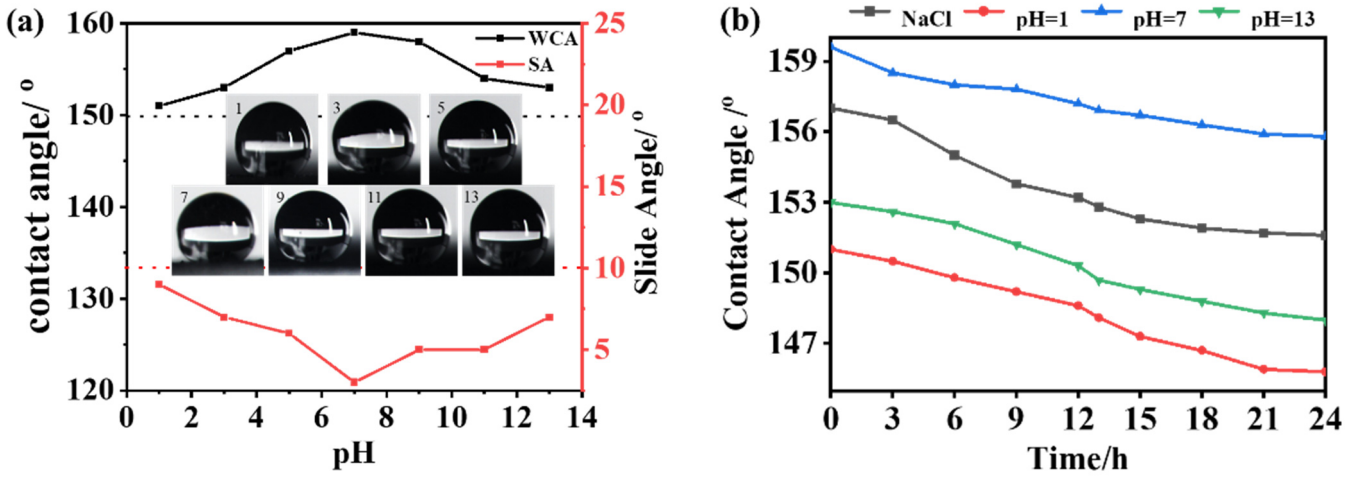

Figure 7. (**a**) Contact angle and rolling angle of CS3-E coating under different pH conditions; (**b**) The change of contact angle with time for CS3-E under different pH conditions.

The durability of coatings with different levels of functionalized nanoparticle doping was evaluated through a tape-stripping test, with the CS3-E coating as the reference. As shown in Figure 8, the contact angle of the coatings decreased as the number of tape peeling cycles increased. In particular, the contact angle for the CS1-E and CS5-E coatings fell below 150° after 120 and 170 rounds of tape peeling, respectively. In stark contrast, the CS3-E coating maintained its superhydrophobic properties even after undergoing 300 cycles of tape peeling. This remarkable durability of the CS3-E coating can be attributed to several key factors: First, the precise ratio of functionalized nanoparticles to epoxy resin contributes to its resilience. Additionally, the strong bond between the nanoparticles and the epoxy matrix, as well as the interlocking of nanoparticles, enhances the overall mechanical stability of the coating. This results in the effective retention of micro- and nanostructures on the surface even after repeated tape peeling. Compared to typical micro- and nanostructured superhydrophobic coatings, the CS3-E coating displayed significantly improved mechanical durability [38–40]. Figure 8b offers a comparison of the mechanical durability of various superhydrophobic surfaces, as reported in recent studies and tested similarly. Notably, among these coatings, the CS3-E, developed in this study, exhibited the highest superhydrophobicity, even after undergoing maximum abrasion cycles [41–52]. This enhanced durability positions it as a promising choice for various applications, including the incorporation of CNTs in carbon nanotube/epoxy composites.

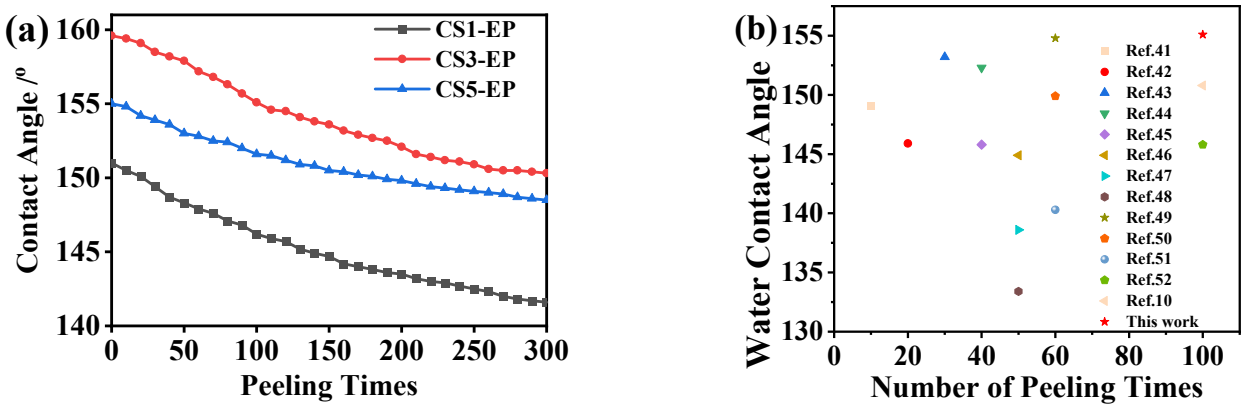

Figure 8. (**a**) The change of coating contact angle with peeling times; (**b**) abrasion cycles and WCAs reported in this work and references [10,41–52].

Several vital variables contribute significantly to the enhanced endurance of CS3-EP coatings. First and foremost, the remarkable mechanical strength of carbon nanotubes (CNTs) plays a pivotal role in bolstering the coating's overall robustness and longevity. This inherent strength makes the coating less susceptible to external forces and less prone to deterioration. Furthermore, introducing SiO_2 imparts an additional layer of protection to the CNTs. This protective layer serves as a shield, safeguarding the CNTs from direct exposure to external forces, such as abrasion and impact. Consequently, it helps to preserve the structural integrity of the CNTs over extended periods. Additionally, the nanoparticles within the coating create an intricate, interlocking structure. This interlocking effect is particularly effective in preventing the functionalized nanoparticle aggregates from detaching or peeling off from the coating's surface when subjected to external forces [25].

3.5. Photothermal and De-Icing Properties

It is widely recognized that thin films containing CNTs exhibit exceptional photothermal characteristics, efficiently converting light energy into heat [53]. To assess the photothermal performance of coatings with varying levels of functionalized nanoparticle doping, we subjected them to simulated solar irradiation, monitoring the temperature near the irradiation spot. The summarized results are presented in Figure 9. The surface temperature of the epoxy coating remained relatively stable, with minimal changes, even

after 100 s of irradiation, settling at approximately 44.3 °C. In contrast, coatings containing functionalized nanoparticles demonstrated a rapid increase in surface temperature during irradiation, reaching a steady level within the same timeframe. The plateau temperatures for the CS1-E, CS3-E, and CS5-E coatings were particularly noteworthy, measuring 80.5 °C, 78.6 °C, and 68.7 °C, respectively. Importantly, the photothermal efficiency exhibited an upward trend with an increasing content of CNTs in the coatings. Given the similarity in surface temperatures between the CS3-E and CS5-E coatings, they emerge as strong candidates for photothermal conversion applications.

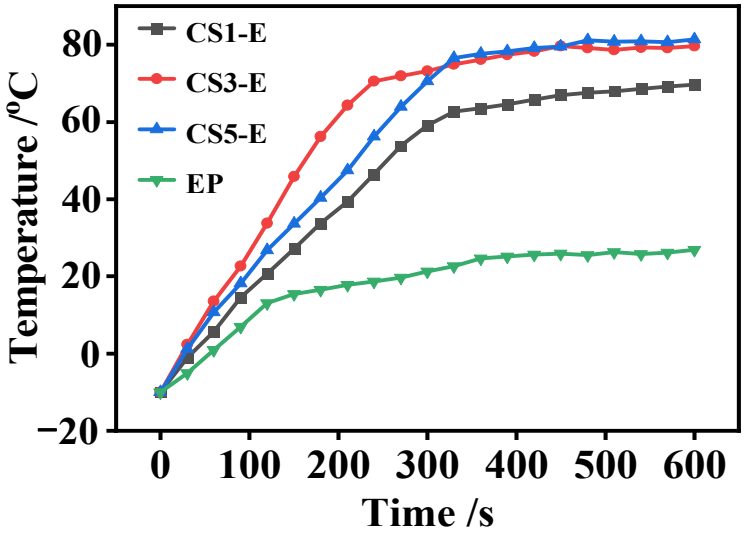

Figure 9. The variation curve of coating temperature with illumination time.

Functionalized nanoparticle coatings offer significant potential for anti-icing and de-icing applications owing to their exceptional photothermal efficiency and superhydrophobic properties. To assess their anti-icing effectiveness, we conducted a test in which 10 μL water droplets were placed on the coated surfaces at a temperature of 20 °C. Figure 10a,c depict the freezing process of these droplets on the CS3-E coating and the uncoated epoxy surface, respectively. On the epoxy surface, the water droplets assumed a semicircular shape and quickly froze, taking only 22 s. In stark contrast, the freezing time on the CS3-E coating was substantially extended to 352 s. Here, the droplets retained their spherical shape, demonstrating outstanding superhydrophobic characteristics. This delay in freezing can be attributed to the significant reduction in the contact area between the water and the superhydrophobic surface, resulting in decreased heat transfer efficiency [54,55]. The 330 s freezing period on the CS3-E coating far exceeded what is typically observed on surfaces lacking superhydrophobic attributes. The apparent micro- and nano-graded structure of the CS3-E surface plays a pivotal role in enhancing its anti-icing performance. To evaluate the de-icing capability of these coatings with photothermal conversion, we employed Xenon light to simulate sunlight irradiation on the surface. Figure 10b illustrates the performance of the CS3-E coating. The ice droplet initiated melting after 417 s and was completely melted within 535 s, thanks to the remarkable photothermal conversion capacity of the carbon nanotubes (CNTs). This exceptional de-icing performance underscores the effectiveness of photothermal conversion in swiftly and efficiently eliminating ice layers from the CS3-E coating. Notably, the droplet did not melt in response to Xenon light alone, emphasizing the specific role played by the photothermal properties of the CNTs in this de-icing process. In summary, these findings underscore the potential of these coatings for anti-icing and de-icing applications. They offer extended anti-icing capabilities and efficient de-icing performance via photothermal conversion.

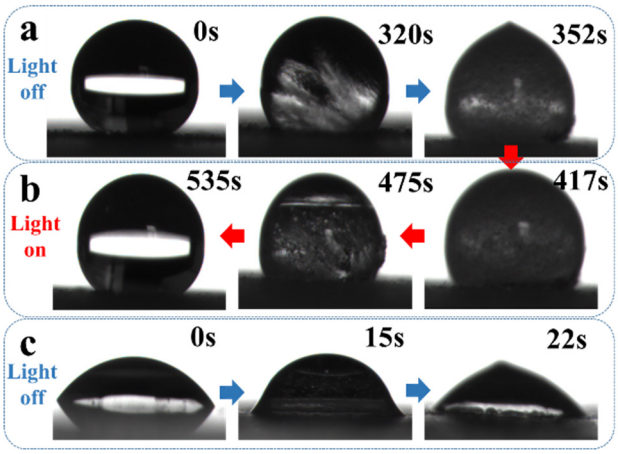

Figure 10. Freezing/melting images of droplets on the coating surface (**a**) CS3-E with light off, (**b**) CS3-E with light off, (**c**) Epoxy resin.

4. Conclusions

In this study, we have successfully engineered a multifunctional superhydrophobic coating, distinguished by its exceptional chemical stability, mechanical robustness, and efficient photothermal conversion capabilities. This innovative coating was formulated using an epoxy matrix combined with functionalized nanoparticles, and it was applied to concrete surfaces using a straightforward and scalable spray-coating method. Notably, the surface morphology and roughness of the CS3-E coatings can be customized by adjusting the ratio of functionalized nanoparticles to epoxy. The CS3-E coating exhibited remarkable hydrophobic characteristics, boasting an impressive water contact angle (WCA) of 159.6°. This coating features a robust micro-nano hierarchical structure, retaining its superhydrophobicity even after enduring extensive tape-peeling damages, thanks to the interwoven structure of functionalized nanoparticles. This durability is a critical asset for practical, real-world applications. Furthermore, our superhydrophobic coating demonstrated excellent photothermal conversion capabilities. It significantly delayed the freezing of water compared to an untreated epoxy coating, showcasing a sixteen-fold improvement in anti-icing performance. Additionally, it efficiently removed ice when subjected to simulated sunlight irradiation. Overall, this research contributes to adopting an inexpensive and simplified surface modification process for CNTs and extends the sustainability of superhydrophobic coatings. While initially designed for cement concrete surfaces, the multifunctional superhydrophobic coatings developed in this study can potentially extend their utility to various industrial applications, particularly in the domains of anti-icing and anti-fogging.

Author Contributions: Conceptualization, S.L. and Y.T.; methodology, Y.L.; software, S.L.; validation, D.Y; formal analysis, J.L.; investigation, D.W.; resources, J.Z.; data curation, S.L.; writing—original draft preparation, S.L.; writing—review and editing, D.Y.; visualization, J.L.; supervision, D.W.; project administration, S.L.; funding acquisition, Y.T. All authors have read and agreed to the published version of the manuscript.

Funding: This research was funded by the National Natural Science Foundation of China joint fund for regional innovation and development (No. U20A20315), Department of Education of Anhui Province (No. RZ2100003733). The authors gratefully acknowledge their financial support.

Institutional Review Board Statement: Not applicable.

Informed Consent Statement: Not applicable.

Data Availability Statement: Access to any other materials can be requested by writing to the corresponding authors.

Conflicts of Interest: The authors declare no conflict of interest.

References

1. Laforte, C.; Tremblay, M.M. Comparative Evaluation of the Anti-Icing Protection Time of Runway Deicers Using Infrared Thermography. *Cold Reg. Sci. Technol.* **2017**, *138*, 57–62. [CrossRef]
2. Arabzadeh, A.; Ceylan, H.; Kim, S.; Gopalakrishnan, K.; Sassani, A.; Sundararajan, S.; Taylor, P.C. Superhydrophobic Coatings on Portland Cement Concrete Surfaces. *Constr. Build. Mater.* **2017**, *141*, 393–401. [CrossRef]
3. Young, L.M.; Durham, S.A. Performance of an Anti-Icing Epoxy Overlay on Asphalt Surfaces. *J. Perform. Constr. Facil.* **2013**, *27*, 836–840. [CrossRef]
4. Yuan, D.; Jiang, W.; Sha, A.; Xiao, J.; Wu, W.; Wang, T. Technology Method and Functional Characteristics of Road Thermoelectric Generator System Based on Seebeck Effect. *Appl. Energy* **2023**, *331*, 120459. [CrossRef]
5. Horgnies, M.; Chen, J.J. Superhydrophobic Concrete Surfaces with Integrated Microtexture. *Cem. Concr. Compos.* **2014**, *52*, 81–90. [CrossRef]
6. Tabatabai, H.; Aljuboori, M. A Novel Concrete-Based Sensor for Detection of Ice and Water on Roads and Bridges. *Sensors* **2017**, *17*, 2912. [CrossRef]
7. Montoya, M.A.; Rahbar-Rastegar, R.; Haddock, J.E. Incorporating Phase Change Materials in Asphalt Pavements to Melt Snow and Ice. *Int. J. Pavement Eng.* **2022**, *23*, 1–14. [CrossRef]
8. Jiang, W.; Yuan, D.; Shan, J.; Ye, W.; Lu, H.; Sha, A. Experimental Study of the Performance of Porous Ultra-Thin Asphalt Overlay. *Int. J. Pavement Eng.* **2022**, *23*, 2049–2061. [CrossRef]
9. Xu, K.; Ren, S.; Song, J.; Liu, J.; Liu, Z.; Sun, J.; Ling, S. Colorful Superhydrophobic Concrete Coating. *Chem. Eng. J.* **2021**, *403*, 126348. [CrossRef]
10. Zhang, F.; Xu, D.; Zhang, D.; Ma, L.; Wang, J.; Huang, Y.; Chen, M.; Qian, H.; Li, X. A Durable and Photothermal Superhydrophobic Coating with Entwinned CNTs-SiO_2 Hybrids for Anti-Icing Applications. *Chem. Eng. J.* **2021**, *423*, 130238. [CrossRef]
11. Hossain, K.; Fu, L.; El-Hakim, M. Determination of Optimum Salting Rates for Asphalt Pavements in a Canadian Climate. *J. Cold Reg. Eng.* **2022**, *36*, 04022003. [CrossRef]
12. Yener, E. A New Frost Salt Scaling Mechanism for Concrete Pavements Based on Brine Rejection from Ice Layer Adhered to Concrete Surface. *Road Mater. Pavement Des.* **2015**, *16*, 89–100. [CrossRef]
13. Abohassan, A.; El-Basyouny, K.; Kwon, T.J. Factors Influencing Pavement Friction during Snowstorms. *J. Cold Reg. Eng.* **2023**, *37*, 04023009. [CrossRef]
14. Heymsfield, E.; Daniels, J.W.; Saunders, R.F.; Kuss, M.L. Developing Anti-Icing Airfield Runways Using Surface Embedded Heat Wires and Renewable Energy. *Sustain. Cities Soc.* **2020**, *52*, 101712. [CrossRef]
15. Jiang, W.; Li, P.; Sha, A.; Li, Y.; Yuan, D.; Xiao, J.; Xing, C. Research on Pavement Traffic Load State Perception Based on the Piezoelectric Effect. *IEEE Trans. Intell. Transp. Syst.* **2023**, *24*, 8264–8278. [CrossRef]
16. Upadhyay, R.K.; Waghmare, P.R. Eco-Friendly Preparation of Superhydrophobic Copper Surfaces for Oil/Water Separation. *Environ. Chem. Lett.* **2020**, *18*, 505–510. [CrossRef]
17. Afrin, S.; Fox, D.; Zhai, L. Organic Superhydrophobic Coatings with Mechanical and Chemical Robustness. *MRS Commun.* **2020**, *10*, 346–352. [CrossRef]
18. Saji, V.S. Carbon Nanostructure-Based Superhydrophobic Surfaces and Coatings. *Nanotechnol. Rev.* **2021**, *10*, 518–571. [CrossRef]
19. Kiraz, A.; Karadag, Y.; Yorulmaz, S.C.; Muradoglu, M. Reversible Photothermal Tuning of a Salty Water Microdroplet. *Phys. Chem. Chem. Phys.* **2009**, *11*, 2597–2600. [CrossRef]
20. Kwak, Y.; Jun, H.Y.; Lee, Y.; Kang, M.; Oh, J.S.; Kim, S.; Song, Y.H.; Choi, C.-H. Multiprocessible and Durable Superhydrophobic Coating Suspension Enabling Printed Patterning, Internal Tubular Coating, and Planar Surface Coating. *Ind. Eng. Chem. Res.* **2021**, *60*, 8743–8752. [CrossRef]
21. Lahiri, S.K.; Zhang, P.; Zhang, C.; Liu, L. Robust Fluorine-Free and Self-Healing Superhydrophobic Coatings by H3BO3 Incorporation with SiO_2–Alkyl-Silane@PDMS on Cotton Fabric. *ACS Appl. Mater. Interfaces* **2019**, *11*, 10262–10275. [CrossRef] [PubMed]
22. Tee, S.Y.; Ye, E.; Teng, C.P.; Tanaka, Y.; Tang, K.Y.; Win, K.Y.; Han, M.-Y. Advances in Photothermal Nanomaterials for Biomedical, Environmental and Energy Applications. *Nanoscale* **2021**, *13*, 14268–14286. [CrossRef] [PubMed]
23. Balou, S.; Shandilya, P.; Priye, A. Carbon Dots for Photothermal Applications. *Front. Chem.* **2022**, *10*, 1023602. [CrossRef] [PubMed]
24. Jiang, G.; Chen, L.; Zhang, S.; Huang, H. Superhydrophobic SiC/CNTs Coatings with Photothermal De-icing and Passive Anti-Icing Properties. *ACS Appl. Mater. Interfaces* **2018**, *10*, 36505–36511. [CrossRef]
25. Liu, Y.; Wu, Y.; Liu, Y.; Xu, R.; Liu, S.; Zhou, F. Robust Photothermal Coating Strategy for Efficient Ice Removal. *ACS Appl. Mater. Interfaces* **2020**, *12*, 46981–46990. [CrossRef]
26. Zhang, L.; Gao, C.; Zhong, L.; Zhu, L.; Chen, H.; Hou, Y.; Zheng, Y. Robust Photothermal Superhydrophobic Coatings with Dual-Size Micro/Nano Structure Enhance Anti-/de-Icing and Chemical Resistance Properties. *Chem. Eng. J.* **2022**, *446*, 137461. [CrossRef]
27. Hooda, A.; Goyat, M.S.; Pandey, J.K.; Kumar, A.; Gupta, R. A Review on Fundamentals, Constraints and Fabrication Techniques of Superhydrophobic Coatings. *Prog. Org. Coat.* **2020**, *142*, 105557. [CrossRef]

28. Nguyen-Tri, P.; Tran, H.N.; Plamondon, C.O.; Tuduri, L.; Vo, D.-V.N.; Nanda, S.; Mishra, A.; Chao, H.-P.; Bajpai, A.K. Recent Progress in the Preparation, Properties and Applications of Superhydrophobic Nano-Based Coatings and Surfaces: A Review. *Prog. Org. Coat.* **2019**, *132*, 235–256. [CrossRef]
29. Wang, L.; Yin, K.; Zhu, Z.; Deng, Q.; Huang, Q. Femtosecond Laser Engraving Micro/Nanostructured Poly (Ether-Ether-Ketone) Surface with Superhydrophobic and Photothermal Ability. *Surf. Interfaces* **2022**, *31*, 102013. [CrossRef]
30. Hussain, S.; Wan, X.; Fang, Z.; Peng, X. Superhydrophilic and Photothermal Fe-TCPP Nanofibrous Membrane for Efficient Oil-in-Water Nanoemulsion Separation. *Langmuir* **2021**, *37*, 12981–12989. [CrossRef]
31. Xie, Z.; Wang, H.; Geng, Y.; Li, M.; Deng, Q.; Tian, Y.; Chen, R.; Zhu, X.; Liao, Q. Carbon-Based Photothermal Superhydrophobic Materials with Hierarchical Structure Enhances the Anti-Icing and Photothermal De-icing Properties. *ACS Appl. Mater. Interfaces* **2021**, *13*, 48308–48321. [CrossRef] [PubMed]
32. Mnoyan, A.; Choi, M.; Hyun Kim, D.; Ku, B.-J.; Kim, H.; Jin Lee, K.; Yasin, A.S.; Nam, S.; Lee, K. Cheap, Facile, and Upscalable Activated Carbon-Based Photothermal Layers for Solar Steam Generation. *RSC Adv.* **2020**, *10*, 42432–42440. [CrossRef] [PubMed]
33. Tian, Y.; Xu, Y.; Zhu, Z.; Liu, Y.; Xie, J.; Zhang, B.; Zhang, H.; Zhang, Q. Hierarchical Micro/Nano/Porous Structure PVDF/Hydrophobic GO Photothermal Membrane with Highly Efficient Anti-Icing/ de-Icing Performance. *Colloid Surf. A-Physicochem. Eng. Asp.* **2022**, *651*, 129586. [CrossRef]
34. Soni, R.; Joshi, S.R.; Karmacharya, M.; Min, H.; Kim, S.-K.; Kumar, S.; Kim, G.-H.; Cho, Y.-K.; Lee, C.Y. Superhydrophobic and Self-Sterilizing Surgical Masks Spray-Coated with Carbon Nanotubes. *ACS Appl. Nano Mater.* **2021**, *4*, 8491–8499. [CrossRef]
35. Dash, S.; de Ruiter, J.; Varanasi, K.K. Photothermal Trap Utilizing Solar Illumination for Ice Mitigation. *Sci. Adv.* **2018**, *4*, eaat0127. [CrossRef]
36. Wang, X.; Dai, L.; Jiao, N.; Tung, S.; Liu, L. Superhydrophobic Photothermal Graphene Composites and Their Functional Applications in Microrobots Swimming at the Air/Water Interface. *Chem. Eng. J.* **2021**, *422*, 129394. [CrossRef]
37. Yeong, Y.H.; Wang, C.; Wynne, K.J.; Gupta, M.C. Oil-Infused Superhydrophobic Silicone Material for Low Ice Adhesion with Long-Term Infusion Stability. *ACS Appl. Mater. Interfaces* **2016**, *8*, 32050–32059. [CrossRef]
38. Tondro, G.H.; Behzadpour, N.; Keykhaee, Z.; Akbari, N.; Sattarahmady, N. Carbon@polypyrrole Nanotubes as a Photosensitizer in Laser Phototherapy of Pseudomonas Aeruginosa. *Colloids Surf. B Biointerfaces* **2019**, *180*, 481–486. [CrossRef]
39. Jamil, M.I.; Zhan, X.; Chen, F.; Cheng, D.; Zhang, Q. Durable and Scalable Candle Soot Icephobic Coating with Nucleation and Fracture Mechanism. *ACS Appl. Mater. Interfaces* **2019**, *11*, 31532–31542. [CrossRef]
40. Niu, H.; Li, J.; Wang, X.; Luo, F.; Qiang, Z.; Ren, J. Solar-Assisted, Fast, and In Situ Recovery of Crude Oil Spill by a Superhydrophobic and Photothermal Sponge. *ACS Appl. Mater. Interfaces* **2021**, *13*, 21175–21185. [CrossRef]
41. Gong, X.; Zhang, L.; He, S.; Jiang, S.; Wang, W.; Wu, Y. Rewritable Superhydrophobic Coatings Fabricated Using Water-Soluble Polyvinyl Alcohol. *Mater. Des.* **2020**, *196*, 109112. [CrossRef]
42. Zhang, B.; Xu, W.; Zhu, Q.; Sun, Y.; Li, Y. Mechanically Robust Superhydrophobic Porous Anodized AA5083 for Marine Corrosion Protection. *Corros. Sci.* **2019**, *158*, 108083. [CrossRef]
43. Masood, M.T.; Heredia-Guerrero, J.A.; Ceseracciu, L.; Palazon, F.; Athanassiou, A.; Bayer, I.S. Superhydrophobic High Impact Polystyrene (HIPS) Nanocomposites with Wear Abrasion Resistance. *Chem. Eng. J.* **2017**, *322*, 10–21. [CrossRef]
44. Luo, X.; Wei, M.; Cao, M.; Ren, H.; Feng, J. Wear-Resistant and Conductive Superhydrophobic Coatings with Nest-like Structure Prepared by a One-Step Spray-Drying Method. *Chem. Eng. Process. -Process Intensif.* **2018**, *131*, 27–33. [CrossRef]
45. Zhang, X.-F.; Chen, Y.-Q.; Hu, J.-M. Robust Superhydrophobic SiO_2/Polydimethylsiloxane Films Coated on Mild Steel for Corrosion Protection. *Corros. Sci.* **2020**, *166*, 108452. [CrossRef]
46. Wang, Z.; Yang, A.; Tan, X.; Tu, Y.; Sabin, S.; Xiang, P.; Wang, M.; Guo, R.; Chen, X. A Veil-over-Sprout Micro-Nano PMMA/SiO_2 Superhydrophobic Coating with Impressive Abrasion, Icing, and Corrosion Resistance. *Colloids Surf. A Physicochem. Eng. Asp.* **2020**, *601*, 124998. [CrossRef]
47. Liu, H.; Geng, W.; Jin, C.-J.; Wu, S.-M.; Lu, Y.; Hu, J.; Yu, H.-Z.; Chang, G.-G.; Zhao, T.; Wan, Y.; et al. Silica Coating with Well-Defined Micro-Nano Hierarchy for Universal and Stable Surface Superhydrophobicity. *Chem. Phys. Lett.* **2019**, *730*, 594–599. [CrossRef]
48. Barthwal, S.; Lim, S.-H. A Durable, Fluorine-Free, and Repairable Superhydrophobic Aluminum Surface with Hierarchical Micro/Nanostructures and Its Application for Continuous Oil-Water Separation. *J. Membr. Sci.* **2021**, *618*, 118716. [CrossRef]
49. Guo, J.; Wang, C.; Yu, H.; Li, X. Preparation of a Wear-Resistant, Superhydrophobic SiO_2/Silicone-Modified Polyurethane Composite Coating through a Two-Step Spraying Method. *Prog. Org. Coat.* **2020**, *146*, 105710. [CrossRef]
50. Qu, M.; Liu, S.; He, J.; Feng, J.; Yao, Y.; Ma, X.; Hou, L.; Liu, X. Fabrication of Recyclable and Durable Superhydrophobic Materials with Wear/Corrosion-Resistance Properties from Kaolin and Polyvinylchloride. *Appl. Surf. Sci.* **2017**, *410*, 299–307. [CrossRef]
51. Xie, J.; Hu, J.; Lin, X.; Fang, L.; Wu, F.; Liao, X.; Luo, H.; Shi, L. Robust and Anti-Corrosive PDMS/SiO_2 Superhydrophobic Coatings Fabricated on Magnesium Alloys with Different-Sized SiO_2 Nanoparticles. *Appl. Surf. Sci.* **2018**, *457*, 870–880. [CrossRef]
52. Xiao, S.; Hao, X.; Yang, Y.; Li, L.; He, N.; Li, H. Feasible Fabrication of a Wear-Resistant Hydrophobic Surface. *Appl. Surf. Sci.* **2019**, *463*, 923–930. [CrossRef]
53. Neelgund, G.M.; Okolie, M.C.; Williams, F.K.; Oki, A. Ag_2S Nanocrystallites Deposited over Polyamidoamine Grafted Carbon Nanotubes: An Efficient NIR Active Photothermal Agent. *Mater. Chem. Phys.* **2019**, *234*, 32–37. [CrossRef] [PubMed]

54. Zigmond, J.S.; Pollack, K.A.; Smedley, S.; Raymond, J.E.; Link, L.A.; Pavía-Sanders, A.; Hickner, M.A.; Wooley, K.L. Investigation of Intricate, Amphiphilic Crosslinked Hyperbranched Fluoropolymers as Anti-Icing Coatings for Extreme Environments. *J. Polym. Sci. Part A Polym. Chem.* **2016**, *54*, 238–244. [CrossRef]
55. Puretskiy, N.; Chanda, J.; Stoychev, G.; Synytska, A.; Ionov, L. Anti-Icing Superhydrophobic Surfaces Based on Core-Shell Fossil Particles. *Adv. Mater. Interfaces* **2015**, *2*, 1500124. [CrossRef]